HHS Public Access

Author manuscript

Theriogenology. Author manuscript; available in PMC 2017 September 11.

Published in final edited form as:

Theriogenology. 2005 June ; 63(9): 2395–2415. doi:10.1016/j.theriogenology.2004.09.051.

A theoretically estimated optimal cooling rate for the cryopreservation of sperm cells from a live-bearing fish, the green swordtail *Xiphophorus helleri*

Sreedhar Thirumala[a], **Changjiang Huang**[b], **Qiaoxiang Dong**[b], **Terrence R. Tiersch**[b], and **Ram V. Devireddy**[a,*]

[a]Bioengineering Laboratory, Department of Mechanical Engineering, Louisiana State University, Baton Rouge, LA, USA

[b]Aquaculture Research Station, Louisiana Agricultural Experiment Station, Louisiana State University Agricultural Center, Baton Rouge, LA, USA

Abstract

Sperm cryopreservation of live-bearing fishes, such as those of the genus *Xiphophorus* is only beginning to be studied, although these fishes are valuable models for biomedical research and are commercially raised as ornamental fish for use in aquariums. To explore optimization of techniques for sperm cryopreservation of these fishes, this study measured the volumetric shrinkage response during freezing of sperm cells of *Xiphophorus helleri* by use of a shape-independent differential scanning calorimeter (DSC) technique. Volumetric shrinkage during freezing of *X. helleri* sperm cell suspensions was obtained in the presence of extracellular ice at a cooling rate of 20 °C/min in three different media: (1) Hanks' balanced salt solution (HBSS) without cryoprotective agents (CPAs); (2) HBSS with 14% (v/v) glycerol; and (3) HBSS with 10% (v/v) dimethyl sulfoxide (DMSO). The sperm cell was modeled as a cylinder of 33.3 μm in length and 0.59 μm in diameter with an osmotically inactive cell volume (V_b) of 0.6 V_o, where V_o is the isotonic or initial cell volume. By fitting a model of water transport to the experimentally determined volumetric shrinkage data, the best-fit membrane permeability parameters (reference membrane permeability to water, L_{pg} or L_{pg}[cpa] and the activation energy, E_{Lp} or E_{Lp}[cpa]) of the *Xiphophorus helleri* sperm cell membrane were determined. The best-fit membrane permeability parameters at 20 °C/min in the absence of CPAs were: $L_{pg} = 0.776 \times 10^{-15}$ m^3/Ns (0.0046 μm/min atm), and $E_{Lp} = 50.1$ kJ/mol (11.97 kcal/mol) ($R^2 = 0.997$). The corresponding parameters in the presence of 14% glycerol were L_{pg}[cpa] = 1.063×10^{-15} m^3/Ns (0.0063 μm/min atm), and E_{Lp}[cpa] = 83.81 kJ/mol (20.04 kcal/mol) ($R^2 = 0.997$). The parameters in the presence of 10% DMSO were L_{pg}[cpa] = 1.4×10^{-15} m^3/Ns (0.0083 μm/min atm), and E_{Lp}[cpa] = 90.96 kJ/mol (21.75 kcal/mol) ($R^2 = 0.996$). Parameters obtained in this study suggested that the optimal rate of cooling for *X. helleri* sperm cells in the presence of CPAs ranged from 20 to 35 °C/min and were in close agreement with recently published, empirically determined optimal cooling rates.

*Corresponding author. Tel.: 1 225 578 5891; fax: +1 225 578 5924. devireddy@me.lsu.edu (R.V. Devireddy).

Keywords

Differential scanning calorimetry; Water transport; Reference membrane permeability and activation energy

1. Introduction

Live-bearing fishes of the genus *Xiphophorus* are widely used in diverse areas of contemporary scientific research, including evolution [1,2], sex determination [3–5], endocrinology [6,7], ethology and behavioral ecology [8–11], toxicology [12,13], parasitology [14,15], immunology [16,17], and cancer genetics [18,19]. In addition to their value as experimental models for biomedical research, swordtails and platyfish are also valued as ornamental fish because of vibrant body coloration and a long sword-like tail. At present, more than 22 species and more than 67 pedigreed lines of *Xiphophorus* are currently maintained only as live animal stocks, perpetuated by a labor-intensive breeding regime (*Xiphophorus* Genetic Stock Center of Texas State University, San Marcos, TX, USA). As new species are identified, new lines developed, and rare chromosomal conditions delineated, it becomes increasingly important to cryogenically preserve *Xiphophorus* sperm samples for the long-term.

Despite the study of sperm cryopreservation in some 200 species of freshwater and marine fishes [20], sperm cryopreservation has only recently been explored in live-bearing fishes as a group [21–23]. The focus of the present study was to measure a biophysical response (water transport) in *X. helleri* sperm cells during freezing using a recent advance in measurement methodology, pioneered by Devireddy and colleagues, using a differential scanning calorimeter (DSC) [24–29]. In the DSC technique, two heat releases from the same cell suspension are measured: (i) during freezing of osmotically active (live) cells in suspension; and (ii) during freezing of osmotically inactive (dead) cells in the same suspension. The difference in heat release measured between the two cooling runs from the same experiment is correlated to water transport. This has been demonstrated by Devireddy and colleagues in a variety of sperm cell suspensions, including murine [24], human [25], equine [26,27], canine [28], boar [29], and recently in an aquatic species, the Pacific oyster *Crassostrea gigas* [30], and independently verified by Yuan and Diller [31] and Diller [32]. As described elsewhere, knowledge of the water transport (cellular dehydration) during freezing of a cell suspension can be used to predict a priori the optimal rates of freezing [24–29,33,34]. Briefly, the loss of post-thaw viability is either due to intracellular ice formation [35,36] or prolonged exposure to freeze-concentrated extracellular solution [37]. Differences in membrane permeability to water and the probability of IIF result in different optimal cooling rates for different cells [34,38]. Therefore, to optimize a cryopreservation protocol, it is important to measure cell membrane permeability to water.

The aim of this project was to establish the water transport (and consequently the membrane permeability parameters) of *X. helleri* sperm during freezing using a DSC technique at a cooling rate of 20 °C/min in three different media: Hanks' balanced salt solution (HBSS) without cryoprotectants; HBSS with 14% glycerol; and HBSS with 10% dimethyl sulfoxide

(DMSO). The experimentally determined membrane permeability parameters were used to numerically predict the loss of intracellular water under a variety of cooling rates (5–100 °C/min). The numerical predictions were analyzed to predict the amount of water left in the sperm cell after dehydration in the absence of IIF, and consequently the optimal cooling rates for *X. helleri* sperm cryopreservation.

2. Materials and methods

2.1. Collection and isolation of sperm cells

A total of 26 male *X. helleri* were shipped weekly by overnight delivery from the *Xiphophorus* Genetic Stock Center (XGSC) of Texas State University (San Marcos, TX, USA) to the Aquaculture Research Station of the Louisiana State University Agricultural Center in January through March of 2004. The fish were anesthetized in 0.01% MS-222 (Western Chemical Inc., Ferndale, WA, USA) for 2 min, and the standard lengths and wet weights were measured. Sperm were collected by surgical removal of the testis, adherent tissue was dissected away and testes were placed in tared resealable plastic bags (NASCO whirl-pak, MBCOCT, New Haven, CT, USA) and weighed [22]. Based on previously published results that report the osmolality of blood plasma of *X. helleri* as 320 mOsm/kg [21–23], HBSS at 300 mOsm/kg was added to the testis before crushing of the testis to release sperm. Sperm concentrations were adjusted to $0.9-1.6\times10^9$ cells/mL, while the motility of fresh sperm always ranged from 80 to 90% motile. The concentration of the cells was adjusted such that the product of initial intracellular cell water (~5 μm^3), the latent heat of fusion of water (335 mJ/mg), the density of intracellular water (1000 kg/m^3) and the number of cells in a DSC sample pan (~ 10^9 cells/mL) translated to a value that could be measured by a DSC-7 machine (Perkin Elmer Corporation, Norwalk, CT, USA) which was 1–3 mJ/mg of sample (see [39] by Devireddy et al. for a more detailed description for the expected value of the DSC heat release). The samples were transported to the LSU bioengineering laboratory for DSC experiments.

2.2. DSC experiments

The DSC experiments were carried out in the absence and presence of CPAs. Nine separate DSC experiments were conducted in the absence of any CPA, in the presence of two CPAs glycerol (14%, v/v) and dimethyl sulfoxide (10%, v/v). Approximately 10 μL of the sperm suspension was loaded in a DSC standard aluminum sample pan (Perkin Elmer Corporation, Norwalk, CT, USA) with ~ 0.5 mg of *Pseudomonas syringae* (ATCC, Rockville, MD, USA). The DSC dynamic cooling protocol used to measure the water transport out of the sperm cells was the same as reported in earlier studies on mammalian [24–29] and aquatic [30] sperm cells and will be briefly stated here. It is important to note that previously published data on *X. helleri* sperm suggested that these cells were “viable” for as long as 2 weeks after collection [22,23]. However, in the interest of consistency all water transport (DSC) experiments were completed within 3–6 h of sperm collection.

2.3. DSC dynamic cooling protocol

Step 1, sperm cell suspensions with or without CPAs initially at room temperature were cooled at 5 °C/min until the extracellular ice nucleated. Step 2, after nucleation, the sample

was thawed at a warming rate (5 °C/min) such that phase-change temperature T_{ph} was reached (but not overshot) and ice remained in the extracellular solution. The phase change temperatures were determined to be − 0.6 °C for the HBSS, − 4.1 °C for HBSS with 14% glycerol, and − 3.2 °C for HBSS with 10% DMSO. Step 3, the sample was cooled to − 50 °C at 20 °C/min causing the sperm cells to undergo dehydration. The lower curve in Fig. 1 corresponds to the heat release associated with dehydration and the total area is represented by $q_{initial}$. Step 4, the sample was re-equilibrated at T_{ph} by thawing at 20 °C/min. Step 5, to differentiate between the heat released by the media and the intracellular fluid in Step 3, the sample was cooled at 200 °C/min to − 150 °C. This caused all the sperm cells to lyse and become osmotically inactive. Step 6, Step 4 was repeated. Step 7, the sample was cooled to − 50 °C at 20 °C/min to measure the final heat release due to lysed (osmotically inactive) sperm cells mixed with media. The upper curve in Fig. 1 corresponds to this heat release and the total area is represented by q_{final}.

Although no independent experiments were conducted as part of this study to assess the viability of the cells prior to the start or during the course of the experiments, that we measured a positive difference in heat release between Step 3 and Step 7 of the DSC cooling protocol described above, confirmed that the cells were osmotically active or intact prior to the start of the DSC experiment. Should the cells be osmotically inactive or lysed prior to the start of the experiment, the DSC cooling protocol will measure no difference in heat release, as described in earlier studies [24–30,39,40]. This assumption is further supported by previously published data [21–23] that suggested that the sperm cells of *X. helleri* remain viable even 2 weeks after collection.

2.4. Translation of heat release to cell volume data for dynamic cooling

The heat release measurements of interest are Δq_{dsc} and $\Delta q(T)_{dsc}$ which are the total and fractional difference between the heat releases measured by integration of the heat flows during freezing of osmotically active (live) cells in media $q_{initial}$, and during freezing of osmotically inactive (dead) cells in media, q_{final}. As defined in a series of earlier studies by Devireddy and colleagues, this difference in heat release has been shown to be related to cell volume changes in several biological systems [24–30,39,40] as:

$$\frac{V_i - V(T)}{V_i - V_f} = \frac{\Delta q(T)_{dsc}}{\Delta q_{dsc}} \quad (1)$$

This equation can be rearranged to measure water transport data from the DSC measured heat releases $\Delta(T)_{dsc}$ and Δq_{dsc} as:

$$V(T) = V_i - \frac{\Delta q(T)_{dsc}}{\Delta q_{dsc}}(V_i - V_f). \quad (2)$$

The unknowns required in Eq. (2) apart from the DSC heat release readings are V_i (the initial cell volume) and V_f (the final cell volume). The initial volume of the sperm cells in the HBSS solution was assumed to be the isotonic cell volume, V_o (~ 9 μm^3) (see Fig. 2 and

Table 1) and from this the initial cell volume, V_i, was calculated to be 1.5 V_o in HBSS with 14% glycerol and 1.35 V_o in HBSS with 10% DMSO. Similarly, the final volume in HBSS was assumed to be the osmotically inactive cell volume, V_b (=0.6 V_o or ~ 5.4 μm^3) and from this the final volume V_f, was calculated to be 0.69 V_i in HBSS with 14% glycerol and 0.67 V_i in HBSS with 10% DMSO.

To ensure the accuracy and repeatability of the experimental data, a set of calibration and control experiments were performed as detailed previously for this instrument (DSC-7, Perkin Elmer Corporation, Norwalk, CT, USA) [39]. One of these tests was to compare the heat release measured during the final cooling run, q_{final}, with the DSC measured heat release from a separate control experiment composed of osmotically inactive (lysed) *X. helleri* spermatozoa; the magnitude (~ 220 mJ/mg) of the heat releases were found to be within ± 1%. This indicated that, after the fast cooling in the DSC protocol (200 °C/min to − 150 °C), the *X. helleri* spermatozoa were osmotically inactive.

2.5. Water transport model

A model for water and solute transport in response to chemical potential gradients based on irreversible thermodynamics has been proposed by Kedem and Katchalsky [41]. The K–K model consisted of two differential equations which describe the water and CPA flux across the membrane [41]. If the flux of CPA is negligible in comparison to the flux of water [42,43], the K–K model reduces to a water transport model, as proposed by Mazur [33] and later modified by Levin et al. [44]. The water transport model of Mazur was further modified [45] to incorporate the presence of CPAs on the volumetric shrinkage response of cells during freezing as:

$$\frac{dV}{dT} = -\frac{L_p A_c R T}{B v_w}\left[1n\frac{(V_o - V_b - n_{cpa}v_{cpa})/v_w}{(V_o - V_b - n_{cpa}v_{cpa})/v_w + (\varphi_s n_s + n_{cpa})} - \frac{\Delta H_f v_w \rho}{R}\left(\frac{1}{T_R} - \frac{1}{T}\right)\right] \quad (3)$$

with L_p, the sperm cell membrane permeability to water defined by Levin et al. [44] as:

$$L_p = L_{pg}[cpa]\exp\left(-\frac{E_{Lp}[cpa]}{R}\left(\frac{1}{T} - \frac{1}{T_R}\right)\right) \quad (4)$$

where, L_{pg}[cpa] is the reference membrane permeability at a reference temperature, T_R (=273.15 K); E_{Lp}[cpa] is the apparent activation energy (kJ/mol) or the temperature dependence of the cell membrane permeability; V is the sperm cell volume at temperature T (K); A_c is the effective membrane surface area for water transport, assumed to be constant during the freezing process; V_o the isotonic (initial) sperm cell volume and V_b is the osmotically inactive cell volume. In this study, the *X. helleri* sperm cell was modeled as a cylinder with length (L) of 33.3 μm and a radius (r_o) of 0.295 μm, which translated to V_o of ~ 9 μm^3 and A_c of ~ 61.7 μm^2 (Table 1 and Fig. 2); R is the universal gas constant; B is the constant cooling rate (K/min); n_{cpa} is the number of moles of salt; v_{cpa} is the molar volume of CPA; v_w is the molar volume of water; φ_s is the disassociation constant for salt; n_s is the

number of osmoles of salt (=$C_i(V_o - V_b)$, where C_i is the initial cell osmolality); ΔH_f is the latent heat of fusion of water, and ρ is the density of water. Note that when n_{cpa} is zero (i.e. no CPA is present), Eqs. (3) and (4) reduce to the water transport model as described by Mazur [33] and Levin et al. [44] and L_p is an Arrhenius function of L_{pg} and E_{Lp}. The two unknown membrane permeability parameters of the model either L_{pg}[cpa] and E_{Lp}[cpa] in the presence of CPA or L_{pg} and E_{Lp} in the absence of CPA, are determined by curve-fitting the water transport model to experimentally obtained volumetric shrinkage data during freezing. The various assumptions made in the development of Mazur's model of water transport are discussed in detail elsewhere [36,40,43,45] and are beyond the scope of this report.

2.6. Numerical methods

A non-linear least squares curve-fitting technique was implemented using a computer program to calculate the membrane permeability parameters that best fit the volumetric shrinkage data as previously described [46]. The optimal fit of Eq. (3) to the experimental data was obtained by selecting a set of parameters that minimized the residual variance, χ^2, and maximized a goodness of fit parameter, R^2 [47]. All of the curve-fitting results presented have an R^2 value ≥ 0.96, indicating that there was good agreement between the experimental data and the fit calculated using the estimated membrane permeability parameters. To simulate the biophysical response of a sperm cell under a variety of cooling rates, the best-fit parameters were substituted in the water transport equation. The water transport equation was then solved numerically using a custom written FORTRAN code (the code utilizes a 4th order Runge–Kutta method) on a Mac Powerbook G4 (Apple Computer Inc., Cupertino, CA, USA) workstation [30,39].

3. Results

3.1. Dynamic cooling response and membrane permeability parameters

The water transport data and simulation using the best-fit parameters in Eq. (3) were measured at a cooling rate of 20 °C/min in HBSS (Fig. 3A), in HBSS with 14% glycerol (Fig. 3B) and in HBSS with 10% DMSO (Fig. 3C). Water transport cessation was observed in the DSC heat release data as an overlap of the thermograms from the heat release signature obtained using osmotically active (initial) and inactive (final) cells (Fig. 1). The dynamic portion of the cooling curve (where the thermograms were distinct) was found to be between − 0.6 and − 10 °C with HBSS, between − 4.1 and − 20 °C with HBSS and 14% glycerol, and between − 3.2 and − 25 °C with HBSS and 10% DMSO. The membrane permeability parameter values that best fit the 20 °C/min water transport data in the absence and presence of CPAs were calculated (Table 2). The model-simulated equilibrium cooling response was generated by setting the left hand side (LHS) of Eq. (3) is equal to 0 and balancing the intracellular and extracellular unfrozen chemical activity of water on the right hand side (RHS) at a particular subzero temperature (shown as a dashed line in Fig. 3).

3.2. Membrane permeability parametric space

The contour plots of the goodness of fit parameter, R^2 (=0.96) in the L_{pg} and E_{Lp} (or L_{pg}[cpa] and E_{Lp}[cpa]) space that corresponds to the water transport data at 20 °C/min in

HBSS (Fig. 4A), in HBSS with 14% glycerol (Fig. 4B), and in HBSS with 10% DMSO (Fig. 4C). Any combination of L_{pg} and E_{Lp} (or L_{pg}[cpa] and E_{Lp}[cpa]) shown to be within the contour was correlated to the water transport data in that media with an R^2 value of >0.96. Note that the contour for the media containing 14% glycerol was almost completely within the contour corresponding to 10% DMSO. This suggested that the membrane permeability parameters obtained in the presence of 10% DMSO could predict the volumetric response of the *X. helleri* sperm cells in the presence of 14% glycerol accurately, while the converse was not true.

3.3. Water transport simulations

Water transport simulations obtained using the best-fit parameters (Table 2) in Eq. (3) are shown for a variety of cooling rates (5–100 °C/min) in Fig. 5. From the simulations, the amount of trapped water (a lower bound on the potential intracellular ice) was computed as a ratio of the volume of the water trapped inside the sperm cell at temperature, T (~ − 30 °C) (where intracellular ice formation could occur by homogenous or volume catalysed nucleation) [36] to the initial sperm water volume, $[(V - V_f)/(V_i - V_f)]$ where V is the volume after water transport ceases (at ~ − 30 °C), V_i is the initial (isotonic) sperm cell volume and V_f is the final (osmotically inactive) sperm cell volume. In the absence of CPAs, for cooling rates of ≤ 60, 80, and 100 °C/min, the trapped water volume was ≤ 0.5, 0.53, and 12.4% of the initial osmotically active water volume, and the corresponding end volumes were ≤ 0.6069 V_i, 0.6071 V_i, and 0.6539 V_i, respectively (Fig. 5A). In the presence of 14% glycerol, for cooling rates of ≤ 20, 40, 60, 80, and 100 °C/min, the trapped water volume was ≤ 2.6, 6.2, 48.3, 59.5, and 66.9% of the initial osmotically active water volume, and the corresponding end volumes were ≤ 0.7027 V_i, 0.7132 V_i, 0.8418 V_i, 0.8761 V_i, and 0.8986 V_i, respectively (Fig. 5B). And finally in the presence of 10% DMSO, for cooling rates of ≤ 20, 40, 60, 80, and 100 °C/min, the trapped water volume was ≤ 1.6, 6.4, 19.6, 51.2, and 59.9% of the initial osmotically active water volume, and the corresponding end volumes were ≤ 0.6824 V_i, 0.6981 V_i, 0.7406 V_i, 0.8425 V_i, and0.8705 V_i, respectively (Fig. 5C).

As described earlier, the cooling rate which optimizes the response to freezing and thawing of any cellular system can be defined as the fastest cooling rate in a given media that proceeds without forming damaging intracellular ice [38]. Generally, intracellular ice formation is defined as damaging and lethal if more than 10–15% of the initial intracellular water is involved [48]. We defined the optimal cooling rate as the rate at which 5% of the initial osmotically active water volume was trapped within the cells at − 30 °C. The simulations (Fig. 5) obtained using the best-fit parameters show that the optimal cooling rate in HBSS as 89 °C/min, in HBSS with 14% glycerol as 29 °C/min, and in HBSS with 10% DMSO as 32 °C/min (Table 2). It is important to note if intracellular ice formation occurs by a heterogeneous or a surface-catalyzed nucleation mechanism [36] (generally between − 5 and − 20 °C for a variety of single cells), which our model does not predict, then potentially even more water would be trapped in the sperm cells than predicted by water transport alone (i.e. the lower bound of intracellular ice discussed above). Thus, the optimal cooling rates (Tables 2 and 3) based on the lower bound of intracellular ice formation would be over-estimated.

3.4. Parameter sensitivity analysis—effect of varying V_b

The value of the osmotically inactive cell volume, V_b of mammalian sperm cells has been reported to be $0.6\,V_o$ (the value used in this and other studies) and to range from as low as $0.23\,V_o$ to as high as $0.75\,V_o$ [24–30,39,40]. To estimate the effect of varying the osmotically inactive cell volume on the measured membrane permeability parameters (L_{pg} and E_{Lp} or L_{pg}[cpa] and E_{Lp}[cpa]), the value of V_b was increased to $0.8\,V_o$ and decreased to $0.4\,V_o$. The DSC data were correspondingly modified (using Eq. (2)) and the modified DSC water transport data were curve fitted to the water transport model (Eqs. (3) and (4)) using the non-linear least squares curve-fitting technique described previously. The predicted values of the membrane permeability parameters (L_{pg} and E_{Lp}) using a value of $0.4\,V_o$ and $0.8\,V_o$ as the osmotically inactive cell volume, are shown in Table 3. Although the predicted membrane permeability parameters using V_b of $0.4\,V_o$ and $0.8\,V_o$ were different from each other and the values obtained using V_b of $0.6\,V_o$ (Table 2), the predicted rates of optimal freezing are not that different and are within ± 20% of one another. Thus, the variation in the value of V_b did not alter our model predicted optimal rates of freezing *X. helleri* sperm cell across a broad range of V_b values. Further studies are clearly needed to understand this lack of sensitivity in the value of the model predicted optimal cooling rates for *X. helleri* sperm cells to the assumed value of V_b.

To further illustrate the effect of varying the osmotically inactive cell volume on the predicted membrane permeability parameters, contour plots (similar to those shown in Fig. 4) were generated for an assumed V_b values of $0.6\,V_o$ and $0.4\,V_o$. A comparison of contour space for the three different values of V_b ($0.4\,V_o$, $0.6\,V_o$, and $0.8\,V_o$) are shown in Fig. 6A (for HBSS with no CPAs), Fig. 6B (HBSS with 14% glycerol), and Fig. 6C (HBSS with 10% DMSO). In the presence of glycerol (Fig. 6B), and DMSO (Fig. 6C) the contour plots obtained with an inactive cell volume of $0.8\,V_o$ were completely enclosed by the contour obtained with an assumed V_b value of $0.6\,V_o$, and a considerable region of the contours obtained with an assumed V_b value of $0.4\,V_o$ were also encompassed by the contours obtained with an assumed V_b value of $0.6\,V_o$. This overlap suggests that the permeability parameters obtained with a V_b value of $0.6\,V_o$ can accurately predict the behavior of *X. helleri* sperm cells with a V_b value of either $0.8\,V_o$ or $0.4\,V_o$, while the converse was not true. However, in the absence of CPAs (Fig. 6A), no precise conclusions could be drawn on the effect of assumed V_b on predicted membrane permeability parameters, although there seemed to be a trend towards lowering the range of best-fit activation energy values (E_{Lp}) with increasing V_b.

3.5. Parameter sensitivity analysis—effect of varying assumed cell dimensions (or surface area to volume ratio)

To account for errors and uncertainities in the measured *X. helleri* sperm cell dimensions, we also investigated the effect of varying the surface area to volume ratio (S:V) by 50% on the predicted membrane permeability parameters. The geometric model was appropriately modified in the water transport model (Eqs. (3) and (4)) and the corresponding best-fit permeability parameters (L_{pg}or L_{pg}[cpa] and E_{Lp} or E_{Lp}[cpa]) were obtained using the non-linear least squares curve-fitting technique as previously described (data not shown). As expected, the membrane permeability parameters obtained by increasing the S:V ratio were

lower than those shown in Tables 2 and 3, and the permeability parameters obtained by decreasing the S:V ratio were higher. This inverse relationship between S:V ratio and the predicted membrane permeability parameters (L_{pg} or L_{pg}[cpa] and E_{Lp} or E_{Lp}[cpa]) was not surprising, because Eq. (3) shows that the change in the cell volume as a function of temperature (dV/dT) is proportional to the product of L_p and A_c. Thus, for a given change in the cell volume as a function of temperature (dV/dT), an increase in A_c (or S:V ratio) will cause a corresponding decrease in the predicted value of L_p, where $L_p = f(L_{pg}, E_{Lp})$ as shown in Eq. (4) and vice-versa. Thus, any changes to the geometrical model of the *X. helleri* sperm cell (specifically membrane surface area, A_c) would manifest themselves with corresponding changes to the membrane permeability parameters predicted by the model (L_{pg} or L_{pg}[cpa] and E_{Lp} or E_{Lp}[cpa]).

Additional numerical simulations were also performed assuming the new S:V ratios and the corresponding water transport parameters in the water transport model (Eqs. (3) and (4)). These simulations were analyzed to predict the optimal cooling rate as described earlier (i.e. the rate at which 5% of the initial osmotically active water volume is trapped within the cells at − 30 °C). The simulations (data not shown) showed that the optimal cooling rate in HBSS as 108 °C/min, in HBSS with 14% glycerol as 24 °C/min, and in HBSS with 10% DMSO as 38 °C/min (for an assumed V_b value of 0.6 V_o and a S:V ratio of 10.2). The corresponding values with an assumed V_b value of 0.6 V_o and a S:V ratio of 3.4 were 72 °C/min (in HBSS), 36 °C/min (in HBSS with 14% glycerol), and 26 °C/min (in HBSS with 10% DMSO). These values are comparable (± 25%) to those obtained earlier using a S:V ratio of 6.8 (Table 2).

4. Discussion

The best-fit parameters obtained in this study using the DSC volumetric shrinkage data during freezing of *X. helleri* spermatozoa appeared to be lower than the reported suprazero (above zero and in the absence of extracellular ice) permeability values for mammalian species [40]. A similar lowering of the sperm cell water permeability parameter values was also found previously by Devireddy and colleagues for mouse [24], human [25], horse [26,27], canine [28], boar [29], and Pacific oyster [30]. This discrepancy between the membrane permeabilities may be associated with possible changes in the sperm cell plasma membrane during suprazero cooling. These changes could include either a lipid phase transition between 0 and 4 °C, or cold shock damage or “chilling” injury during cooling. The presence of extracellular ice further alters the cell membrane transport properties [43,45]. In general, for mammalian cells, the average activation energy obtained in the presence of extracellular ice is approximately twice as large as that for studies conducted in unfrozen solutions at higher temperatures [43]. These changes in membrane transport properties might be associated with a variety of thermotropic (temperature dependent) phase phenomena. For example, the temperature reduction that induces solidification in the extracellular medium may lead to lyotropic (i.e. independent of cooling rate) membrane phase changes and corresponding alterations of water transport and also membrane fluidity [40]. Further studies are needed to elucidate the precise mechanism by which extracellular ice alter membranes during a freezing process.

A comparison of the membrane permeability parameters reported earlier for *C. gigas* sperm cells in the presence of HBSS (1000 mOsm/kg) and 8% DMSO [30] with the values obtained in the present study for *X. helleri* sperm cells in the presence of HBSS (300 mOsm/kg) and 10% DMSO revealed the following differences: the apparent activation energies (different by a factor of 2) and the reference membrane permeability (different by a factor of 4) were higher for *X. helleri* sperm cells. Additionally, the reported optimal rates of freezing of *C. gigas* haploid and diploid sperm cells (~53 °C/min and ~44 °C/min) with 8% DMSO were higher (~27–40%) than the corresponding values with 10% DMSO for *X. helleri* sperm cells (23–32 °C/min). Clearly, the relative importance of the effect of extracellular ice and concentration of CPAs on the predicted membrane permeability parameters (L_{pg} or L_{pg}[cpa] and E_{Lp} or E_{Lp}[cpa]) and on the optimal rates of cooling is dependent on the cell type and the choice of freezing media.

The DSC technique was used to obtain water transport data and water permeability parameters (L_{pg} or L_{pg}[cpa] and E_{Lp} or E_{Lp}[cpa]) of *X. helleri* sperm cells in three different cryoprotective media. There was a large increase (35–80%) in the measured value of reference membrane permeability, L_{pg} (or L_{pg}[cpa]) and the activation energy, E_{Lp} (or E_{Lp}[cpa]) obtained in the presence and absence of CPAs (with an assumed V_b values of $0.6\,V_o$ (Table 2) or $0.4\,V_o$ (Table 3). However, when the assumed value was increased to $0.8\,V_o$, the converse was found to be true, i.e. adding either glycerol or DMSO decreased (~35%) the measured value of the activation energy, E_{Lp} (or E_{Lp}[cpa]) while the values of reference membrane permeability, L_{pg} (or L_{pg}[cpa]) were not effected either due to the addition of glycerol (a difference of 3%) or DMSO (a difference of 7%) when compared to values obtained in the absence of CPAs (Table 3).

The best-fit permeability parameters were incorporated into a model of water transport to predict optimal cooling rates for *X. helleri* sperm cells (Tables 2 and 3). The optimal rates in the presence of 14% glycerol or 10% DMSO were smaller (~70%) than the predicted optimal values in their absence. This is surprising, as the presence of CPAs would be expected to increase the ability of the cell membrane to dehydrate at faster cooling rates as shown for mouse and human sperm cell suspensions [24,25] and mammalian (rat) hepatocytes [45]. However, a decrease in the predicted optimal cooling rates in the presence of CPAs was observed in sperm cells of stallion [26], boar [29], and Pacific oyster [30]. Further studies are needed to elucidate the precise mechanism by which CPAs alter membranes during and after freezing and thawing process.

The predicted optimal rates of freezing *X. helleri* sperm cells obtained in the present study ranged from 71 to 90 °C/min in HBSS, 20 to 30 °C/min in HBSS with 14% glycerol, and 24 to 32 °C/min in HBSS with 10% DMSO (Tables 2 and 3). The optimal values in HBSS with 14% glycerol were comparable to the experimentally determined optimal rate of freezing reported recently for *X. helleri* sperm cells [23]. The highest post-thaw motility occurred when the *X. helleri* sperm cells were suspended in HBSS with 14% glycerol were cooled at rates ranging from 20 to 35 °C/min from 5 to −80 °C before plunging into liquid nitrogen, and thawed at 40 °C in a water bath for 7 s [23]. However, Huang et al. [23] reported the highest post-thaw motility (~77%) at a cooling rate of 20 °C/min. This cooling rates is lower (~30%) than the optimal rate obtained assuming $V_b = 0.6\,V_o$ (Table 2) and close (~2%) to

the predicted optimal cooling rate assuming $V_b = 0.8\,V_o$ (Table 3). As stated earlier, the predicted optimal rates using our model are probably over-estimated due to the non-inclusion of heterogeneous or a surface-catalyzed nucleation mechanism. Clearly, the close agreement between the numerically predicted and empirically determined optimal rate of freezing suggests that the membrane permeability parameters presented in this study will help to establish cryopreservation of *X. helleri* sperm cells on a firm biophysical basis.

In conclusion, the water transport (volumetric shrinkage) data for *X. helleri* sperm cells in the presence of extracellular ice and CPAs (glycerol and DMSO) during freezing was obtained in this study using the DSC technique at a cooling rate of 20 °C/min. The measured water transport data in the presence and absence of CPAs was curve-fitted to a model of water transport (Eqs. (3) and (4)), to predict membrane permeability parameters (L_{pg} and E_{Lp} or L_{pg}[cpa] and E_{Lp}[cpa]). The measured "best fit" permeability parameters ranged from, $L_{pg} = 0.409 \times 10^{-15}$ to 2.47×10^{-15} m^3/Ns (0.0024–0.0145 μm/min atm) and E_{Lp} = 41.65–118.98 kJ/mol (9.96–28.45 kcal/mol). The permeability parameters obtained in this study predict an optimal rate of freezing for *X. helleri* sperm cells ranging from 20 to 35 °C/min, which agrees with empirically determined optimal experimental rate (20 °C/min) of freezing *X. helleri* sperm cells [23].

Acknowledgments

This work was supported in part by a grant from the Louisiana Board of Regents (LEQSF 2002-05-RD-A-03) to RD, and grants from the National Institutes of Health and the USDA-SBIR program to TRT. This manuscript was approved for publication by the Director of the Louisiana Agricultural Experiment Station as manuscript number 04-11-0491.

References

1. Meyer A. The evolution of sexually selected traits in male swordtail fishes (*Xiphophorus*:Poeciliidae). Heredity. 1997; 79:329–37.
2. Meyer A, Morrissey JM, Schartl M. Recurrent origin of a sexually selected trait in *Xiphophorus* fishes inferred from a molecular phylogeny. Nature. 1994; 368:539–42. [PubMed: 8139686]
3. Kallman KD. The sex determining mechanism of the poeciliid fish, *Xiphophorus montezumae*, and the genetic control of the sexual maturation process and adult size. Copeia. 1983; 3:755–69.
4. Kallman, KD. A new look at sex determination in poeciliid fishes. In: Turner, BJ., editor. Evolutionary genetics of fishes. New York: Plenum Publishing Corporation; 1984. p. 95-171.
5. Tiersch TR, Chandler RW, Kallman KD, Wachtel SS. Estimation of nuclear DNA content by flow cytometry in fishes of the genus *Xiphophorus*. Comp Biochem Physiol B. 1989; 94:465–8. [PubMed: 2620491]
6. Breuckmann A, Paris F, Schreibman Martin P, Bluem V. Immunoreactive gonadotropin-releasing hormone (GnRH) in the brain and pituitary of adult and juvenile swordtails (*Xiphophorus helleri*, Teleostei, Poeciliidae). J Morphol. 1996; 230:55–67.
7. Flynn KM, Schreibman MP, Yablonsky-Alter E, Banerjee SP. Sexually dimorphic development and binding characteristics of NMDA receptors in the brain of the platyfish. Gen Comp Endocrinol. 1999; 115:282–91. [PubMed: 10417241]
8. Beaugrand JP, Goulet C. Distinguishing kinds of prior dominance and subordination experiences in males of green swordtail fish (*Xiphophorus helleri*). Behav Processes. 2000; 50:131–42. [PubMed: 10969190]
9. Hoefler CD, Morris MR. A technique for the temporary application and augmentation of pigment patterns in fish. Ethology. 1999; 105:431–8.

10. Rosenthal GG, Evans CS. Female preference for swords in *Xiphophorus helleri* reflects a bias for large apparent size. Proc Natl Acad Sci USA. 1998; 95:4431–6. [PubMed: 9539754]
11. Trainor BC, Basolo AL. An evaluation of video playback using *Xiphophorus helleri*. Anim Behav. 2000; 59:83–9. [PubMed: 10640369]
12. De Wolf W, Seinen W, Hermens JLM. N-Acetyltransferase activity in rainbow trout liver and in vitro biotransformation of chlorinated anilines and benzenes in fish. Xenobiotica. 1993; 23:1045–56. [PubMed: 8291263]
13. Paris F, Paassen U, Bluem V. Sperm storage of the female swordtail (*Xiphophorus helleri*). Verh Ges Ichthyol. 1998; 1:157–65.
14. Dove AD. Richness patterns in the parasite communities of exotic poeciliid fishes. Parasitology. 2000; 120:609–23. [PubMed: 10874724]
15. Schmahl G, Schmidt H, Ritter G. The control of ichthyophthiriasis by a medicated food containing quinine: efficacy tests and ultrastructure investigations. Parasitol Res. 1996; 82:697–705. [PubMed: 8897504]
16. Hogarth PJ. Protection of the developing foetus from immunological attack in *Xiphophorus helleri*. J Reprod Fertil. 1970; 23:532. [PubMed: 5492036]
17. McConnell TJ, Godwin UB, Norton SF, Nairn RS, Kazianis S, Morizot DC. Identification and mapping of two divergent, unlinked major histocompatibility complex class II B genes in *Xiphophorus* fishes. Genetics. 1998; 149:1921–34. [PubMed: 9691047]
18. Schartl M. Platyfish and swordtails: a genetic system for the analysis of molecular mechanisms in tumor formation. Trends Genet. 1995; 11:185–9. [PubMed: 7785077]
19. Nairn RS, Kazianis S, McEntire BB, Della CL, Walter RB, Morizot DC. A CDKN2-like polymorphism in *Xiphophorus* LG V is associated with UV-B-induced melanoma formation in platyfish-swordtail hybrids. Proc Natl Acad Sci USA. 1996; 93:13042–7. [PubMed: 8917541]
20. Rana KJ. Cryopreservation of fish spermatozoa Cryopreservation and freeze-drying protocols. Methods Mol Biol. 1995; 38:151–65. [PubMed: 7647854]
21. Huang C, Dong Q, Tiersch TR. Sperm cryopreservation of a live-bearing fish, the platyfish *Xiphophorus* couchianus. Theriogenology. 2004; 62:971–89. [PubMed: 15289041]
22. Huang C, Dong Q, Walter RB, Tiersch TR. Initial studies on sperm cryopreservation of a live bearing fish, the green swordtail *Xiphophorus helleri*. Theriogenology. 2004; 62:179–94. [PubMed: 15159112]
23. Huang C, Dong Q, Walter RB, Tiersch TR. Sperm cryopreservation of green swordtail *Xiphophorus helleri*, a fish with internal fertilization. Cryobiology. 2004; 48:295–308. [PubMed: 15157778]
24. Devireddy RV, Swanlund DJ, Roberts KP, Bischof JC. Sub-zero water permeability parameters of mouse spermatozoa in the presence of extracellular ice and cryoprotective agents. Biol Reprod. 1999; 61:764–75. [PubMed: 10456855]
25. Devireddy RV, Swanlund DJ, Roberts KP, Pryor JL, Bischof JC. The effect of extracellular ice and cryoprotective agents on the water permeability parameters of human sperm plasma membrane during freezing. Hum Reprod. 2000; 15:1125–35. [PubMed: 10783365]
26. Devireddy RV, Olin T, Swanlund DJ, et al. Cryopreservation of equine spermatozoa: optimal cooling rates in the presence and absence of cryoprotective agents. Biol Reprod. 2002; 66:222–31. [PubMed: 11751286]
27. Devireddy RV, Swanlund DJ, Alghamdi AS, et al. Measured effect of collection and cooling conditions on the motility and the water transport parameters at subzero temperatures of equine spermatozoa. Reproduction. 2002; 124:643–8. [PubMed: 12417002]
28. Thirumala S, Ferrer MS, Al-Jarrah A, Eilts BE, Paccamonti DL, Devireddy RV. Cryopreservation of canine spermatozoa: theoretical prediction of optimal cooling rates in the presence and absence of cryoprotective agents. Cryobiology. 2003; 47:109–24. [PubMed: 14580846]
29. Devireddy RV, Fahrig B, Godke RA, Leibo SP. Subzero water transport characteristics of boar spermatozoa confirm observed optimal cooling rates. Mol Reprod Dev. 2004; 67:446–57. [PubMed: 14991736]

30. He Y, Dong Q, Tiersch TR, Devireddy RV. Variation in the membrane transport properties and predicted optimal rates of freezing for spermatozoa of diploid and tetraploid pacific oyster *Crassostrea gigas*. Biol Reprod. 2004; 70:1428–37. [PubMed: 14736816]
31. Yuan S, Diller KR. Study of freezing biological systems using optical differential scanning calorimeter. Proceedings of ASME summer BED conference. 2001; 50:117–8.
32. Diller KR. New techniques in cryomicroscopy. Cryobiology. 2002; 45:250–1.
33. Mazur P. Kinetics of water loss from cells at subzero temperatures and the likelihood of intracellular freezing. J Gen Physiol. 1963; 47:347–69. [PubMed: 14085017]
34. Mazur P. Cryobiology: the freezing of biological systems. Science. 1970; 168:939–49. [PubMed: 5462399]
35. Meryman, HT. Review of biological freezing. In: Meryman, HT., editor. Cryobiology. New York: Academic Press; 1966. p. 1-114.
36. Toner, M. Nucleation of ice crystals in biological cells. In: Steponkus, PL., editor. Advances in low-temperature biology. Greenwich: JAI Press; 1993. p. 1-52.
37. Lovelock JE. Haemolysis of human red blood-cells by freezing and thawing. Biochim Biophys Acta. 1953; 10:414–26. [PubMed: 13058999]
38. Mazur P, Leibo SP, Chu EHY. A two-factor hypothesis of freezing injury. Exp Cell Res. 1972; 71:255–345.
39. Devireddy RV, Raha D, Bischof JC. Measurement of water transport during freezing in cell suspensions using a differential scanning calorimeter. Cryobiology. 1998; 36:124–55. [PubMed: 9527874]
40. Devireddy, RV., Bischof, JC. Recent advances in cryobiology using calorimetry. In: Kakac, S.Smirnov, H., Mila, MR., editors. Low temperature and cryogenic refrigeration. Dordrecht, The Netherlands: Kluwer Academic Publishers; 2003. p. 265-94.
41. Kedem O. Katchalsky Thermodynamic analysis of the permeability of biological membranes to non-electrolytes. Biochim Biophys Acta. 1958; 27:229–46. [PubMed: 13522722]
42. McCaa C, Diller KR, Aggarawal SJ, Takahashi T. Cryomicroscopic determination of the membrane osmotic properties of human monocytes at subfreezing temperatures. Cryobiology. 1991; 28:391–9. [PubMed: 1935177]
43. McGrath, JJ. Membrane transport properties. In: McGrath, JJ., Diller, KR., editors. Low temperature biotechnology: emerging applications and engineering contributions. New York: ASME Press; 1988. p. 273-330.
44. Levin RL, Cravalho EG, Huggins CG. A membrane model describing the effect of temperature on the water conductivity of erythrocyte membranes at subzero temperatures. Cryobiology. 1976; 13:415–29. [PubMed: 971586]
45. Smith DJ, Schulte M, Bischof JC. The effect of dimethylsulfoxide on the water transport response of rat hepatocytes during freezing. ASME J Biomech Eng. 1998; 120:549–58.
46. Bevington, PR., Robinson, DK. Data reduction and error analysis for the physical sciences. New York: McGraw-Hill; 1992. p. 107-24.
47. Montgomery, DC., Runger, GC. Applied statistics and probability for engineers. New York: John Wiley & Sons Inc; 1994. p. 471-529.
48. Mazur P. Equilibrium, quasi-equilibrium, and nonequilibrium freezing of mammalian embryos. Cell Biophys. 1990; 17:53–92. [review]. [PubMed: 1704816]

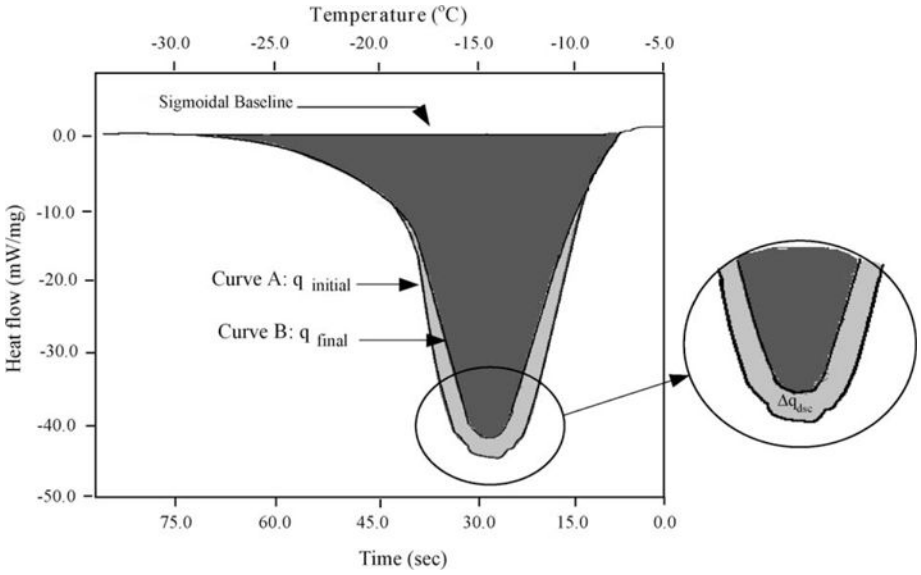

Fig. 1.

Superimposed heat flow thermograms obtained during the initial (osmotically active cells; Curve A) and final (osmotically inactive cells; Curve B) cooling trials of *X. helleri* sperm cells at 20 °C/min obtained in the presence of DMSO. The negative values on the *y*-axis for the heat flow implies an exothermic heat release in the DSC sample. The heat flow (mW/mg) is plotted along the *y*-axis and the sub-zero temperatures (°C) are plotted along the top *x*-axis and time (s) is plotted on the bottom *x*-axis.

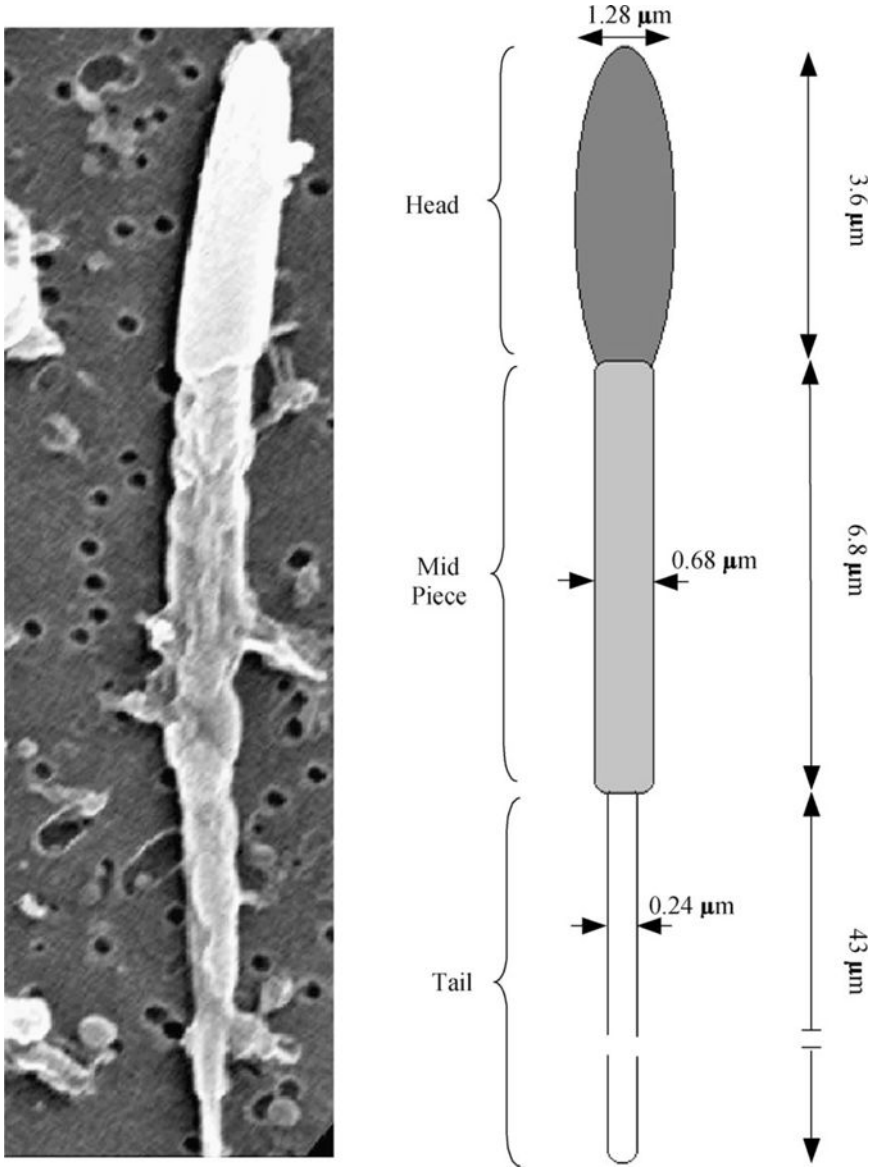

Fig. 2.

Left, representative scanning electron micrographs (SEM) of sperm from *X. helleri* showing the relationship of sperm head and tail in alignment with model used to calculate the cell volumes and surface areas shown on the right. Right, the "geometric" model used to calculate the *X. helleri* sperm cell volumes and surface areas from the SEM images shown on the left.

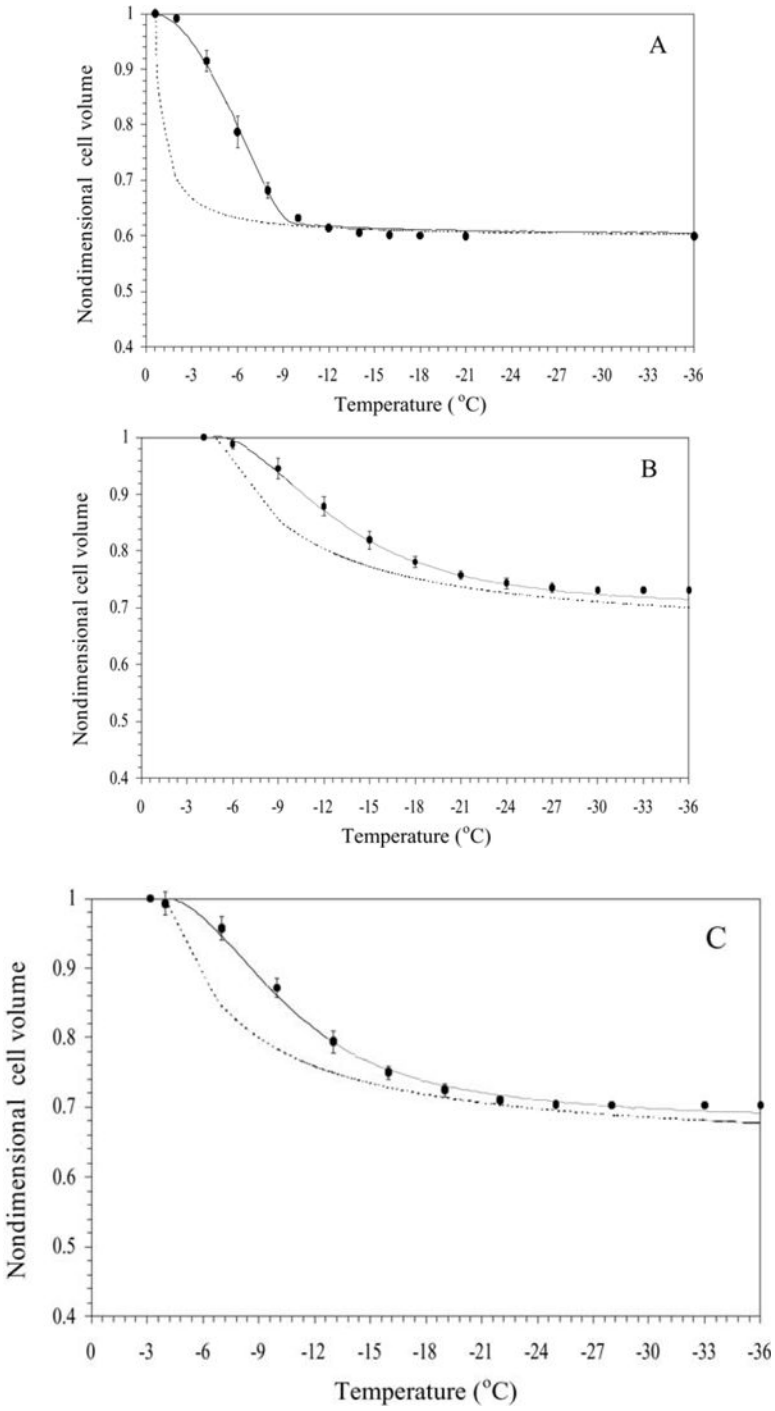

Fig. 3.

Volumetric response of *X. helleri* sperm cells as a function of sub-zero temperatures obtained using the DSC technique in the presence of extracellular ice (A), in the presence of extracellular ice and glycerol (B), and in the presence of extracellular ice and DMSO (C). The filled circles represent the experimentally obtained water transport (volumetric shrinkage) at a cooling rate of 20 °C/min. The dynamic cooling response at 20 °C/min is shown as a solid line and was obtained by using the “best fit” membrane permeability

parameters (L_{pg} and E_{Lp} or L_{pg}[cpa] and E_{Lp}[cpa]) (Table 1) in the water transport equation (Eqs. (3) and (4)). The model-simulated equilibrium cooling response obtained is shown as a dotted line in all the figures. The non-dimensional cell volume is plotted along the *y*-axis and the sub-zero temperatures are shown along the *x*-axis. The error bars represent the standard deviation for the mean values of nine separate DSC experiments ($n = 9$).

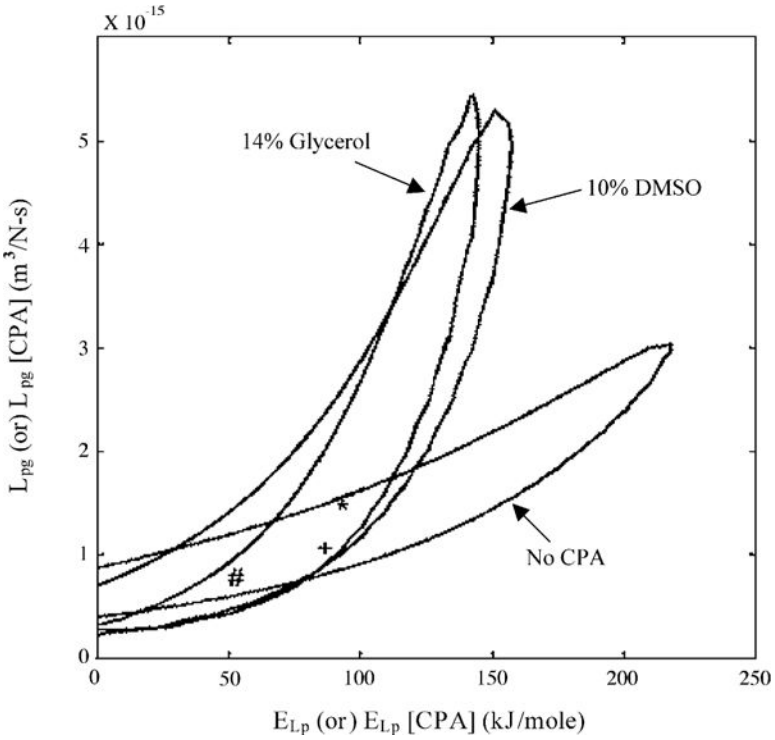

Fig. 4.

Contour plots of the goodness of fit parameter R^2 (= 0.96) for water transport response in *X. helleri* sperm cells in three different media: HBSS with no CPAs (A), HBSS with 14% glycerol (B), and HBSS with 10% DMSO (C). Note that the best-fit parameters (Table 2) are represented within the contours by a "#" (absence of CPAs), "+" (with 14% glycerol) and "*" (with 10% DMSO). The membrane permeability at 0 °C, L_{pg} (or L_{pg}[cpa]) (m^3/Ns) is plotted on the *y*-axis while the apparent activation energy of the membrane, E_{Lp} (or E_{Lp}[cpa]) (kJ/mol) is plotted on the *x*-axis.

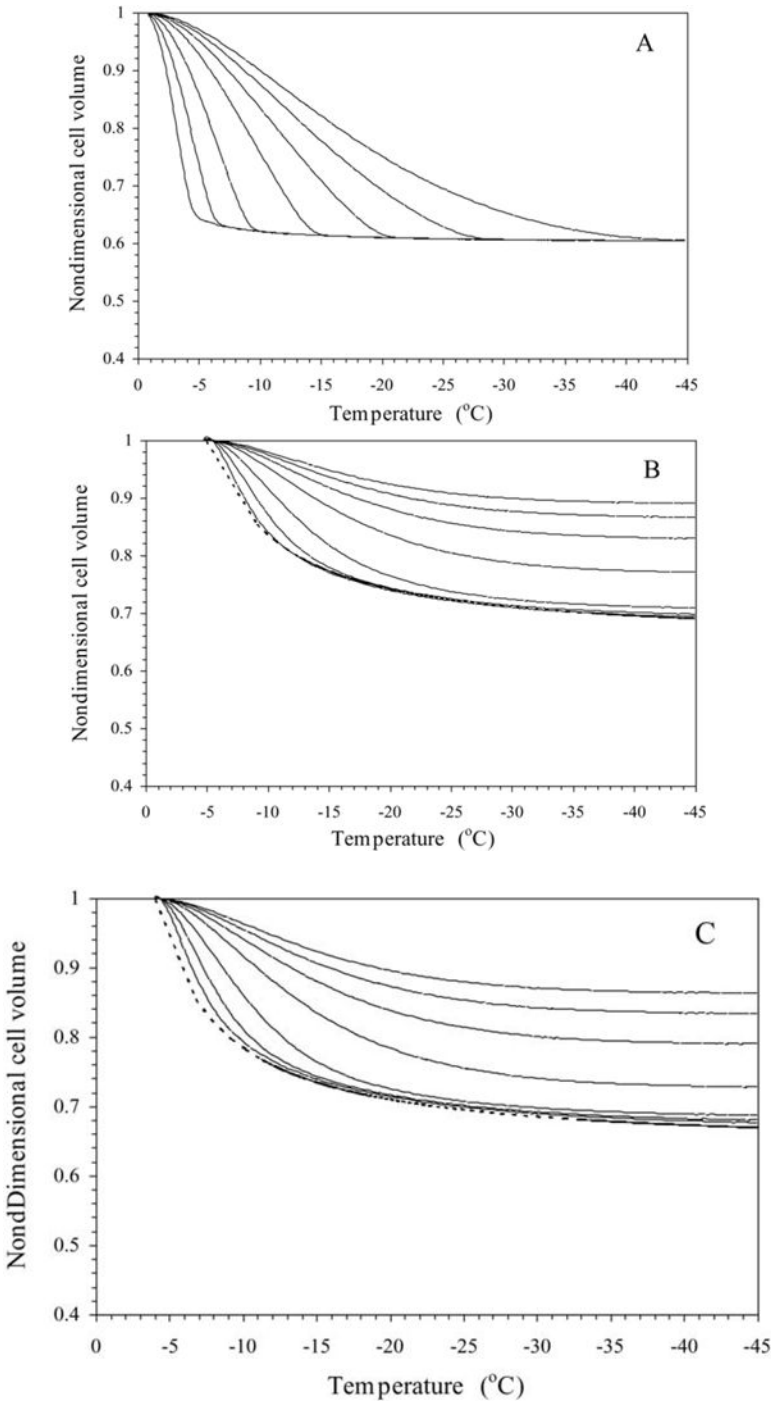

Fig. 5.

Volumetric response of *X. helleri* sperm cells at various cooling rates as a function of sub-zero temperature using the best-fit membrane permeability parameters (Table 1). The changes in the normalized cell volume (V/V_o) are shown as a function of temperature for different cooling rates in *X. helleri* sperm cell suspensions without CPAs (A), with 14% glycerol (B), and with 10% DMSO (C). The water transport curves represent the model-simulated response for different cooling rates (from left to right: 5, 10, 20, 40, 60, 80, and

100 °C/min). The model-simulated equilibrium cooling response obtained is shown as a dotted line. The sub-zero temperatures are shown along the *x*-axis while the non-dimensional volume is plotted along the *y*-axis.

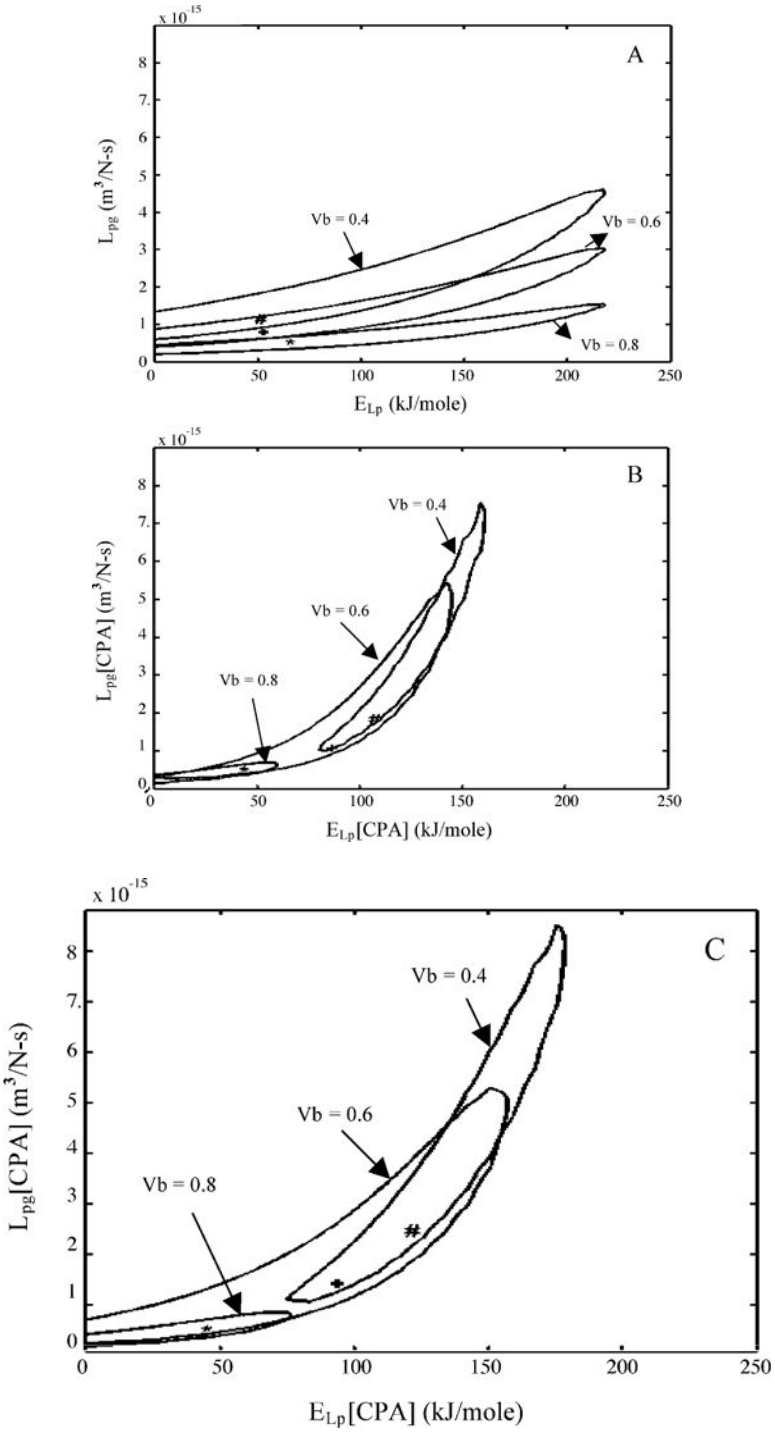

Fig. 6.

Contour plots of the goodness of fit parameter R^2 (= 0.96) for water transport response in *X. helleri* sperm cells in three different media: HBSS with no CPAs (A), HBSS with 14% glycerol (B), and HBSS with 10% DMSO (C). Within each figure, the three contour correspond to the three assumed values of osmotically inactive cell volume, V_b (0.4 V_o, 0.6 V_o, and 0.8 V_o). Note that the best-fit parameters (Tables 2 and 3) are represented within

the contours by a "#" ($V_b = 0.4\,V_o$), "+" ($V_b = 0.6\,V_o$) and "*" ($V_b = 0.8\,V_o$). The membrane permeability at 0 °C, L_{pg} (or L_{pg}[cpa]) (m^3/Ns) is plotted on the *y*-axis while the apparent activation energy of the membrane, E_{Lp} (or E_{Lp}[cpa]) (kJ/mol) is plotted on the *x*-axis.

Table 1

Measurements, and calculated volumes, surface areas, and ratios of surface area to volume (*S*: *V*) for head, midpiece, tail, and combined total of sperm cells from *X. helleri* (*n* = 6)

Sperm cell geometry	Diameter (μm)	Length (μm)	Mean volume (*V*) (μm^3)	Mean surface area (*S*) (μm^2)	*S*:*V* (μm^{-1})
Head[a]	1.28 ± 0.2	3.6 ± 0.4	4.6	14.70	3.07
Mid-piece[a]	0.68 ± 0.1	6.8 ± 0.5	2.5	14.53	5.88
Tail[a]	0.24 ± 0.05	43.0 ± 2.2	1.95	32.42	16.62
Total[b]			9.05	61.65	6.81

[a]The volumes of the head, mid-piece and tail are all assumed to be cylinders.

[b]Sum of the volumes and surface areas of the head, the mid-piece and the tail. Note that as long as the *S*: *V* is maintained as close to the original values as possible, any geometry can be assumed for the sperm cell—for simplicity we assumed the *X. helleri* can be modeled as a thin, long cylinder of length 33.3 μm and a diameter of 0.59 μm (which results in a surface area to volume ratio of 6.78 or within 0.4% of the calculated value). Also see Section 3.5.

Table 2

Predicted sub-zero membrane permeability parameters (the reference membrane permeability in the absence and presence of CPAs, L_{pg} or L_{pg}[cpa] shown in Column 3 and the activation energy in the absence and presence of CPAs, E_{Lp} or E_{Lp}[cpa] shown in Column 4; see text for further description) and the optimal rates of freezing for *X. helleri* sperm cells in the presence of extracellular ice and cryoprotective agents (CPAs)

Assumed inactive cell volume (V_b)	Freezing media	L_{pg} or L_{pg}[cpa] × 10^{15} m^3/Ns (μm/min atm)	E_{Lp} or E_{Lp}[cpa] kJ/mol (kcal/mol)	Goodness of fit, R^2 value[b]	Predicted optimal cooling rate °C/min)[c]
0.6 V_o	HBSS[a]	0.78 (0.0046)	50.10 (11.97)	0.997	89
	HBSS with 14% glycerol[a]	1.06 (0.0063)	83.80 (20.04)	0.997	29
	HBSS with 10% DMSO[a]	1.40 (0.0083)	91.00 (21.75)	0.996	32

[a] Hanks balanced salt solution (300 mOsm/kg) which is physiologically isotonic for *X. helleri* sperm.

[b] A value of 1.0 represents a "perfect" fit between the experimentally measured water transport data and the model-simulated water transport response.

[c] As described in the text "the optimal rate of freezing" is defined as the cooling rate which "traps" 5% of the initial water volume inside the cell at −30 °C.

Table 3

Predicted sub-zero membrane permeability parameters and the optimal rates of freezing for *X. helleri* sperm cells in the presence of extracellular ice and cryoprotective agents (CPAs)

Assumed inactive cell volume (V_b)	Freezing media	L_{pg} or L_{pg}[cpa] × 10^{15} m^3/Ns (μm/min atm)	E_{Lp} or E_{Lp}[cpa] kJ/mol (kcal/mol)	Goodness of fit, R^2 value	Predicted optimal cooling rate (°C/min)
0.4 V_o	HBSS	1.13 (0.0067)	48.90 (11.68)	0.997	90
	HBSS with 14% glycerol	1.82 (0.0108)	104.60 (25.01)	0.997	25
	HBSS with 10% DMSO	2.45 (0.0145)	119.00 (28.45)	0.997	24
0.8 V_o	HBSS	0.42 (0.0025)	62.70 (15.00)	0.996	71
	HBSS with 14% glycerol	0.41 (0.0024)	41.70 (9.96)	0.962	20
	HBSS with 10% DMSO	0.46 (0.0027)	43.20 (10.32)	0.966	25